A Run-Group Proposal Submitted to PAC 44

Measurement of Deep Exclusive π^- Production using a Transversely Polarized ^{3}He Target and the SoLID Spectrometer

DRAFT: May 10, 2016

J. Arrington, K. Hafidi, P. Reimer, Z. Ye*

Argonne National Laboratory, Physics Division, Argonne, IL

H. Gao, X. Li, T. Liu, C. Peng, W. Xiong, X.F. Yan, Z. Zhao

Duke University, Durham, NC 27708, USA

E. Voutier

Institut de Physique Nucléaire IN2P3/CNRS, Université Paris Sud, 91406 Orsay, France

A. Camsonne, J-P. Chen, D. Gaskell

Jefferson Lab, Newport News, VA 23606, USA

M. Boer

Los Alamos National Laboratory, Physics Division, Los Alamos, NM

D. Dutta, L. Ye

Mississippi State University, Department of Physics, MS

C. E. Hyde

Old Dominion University, Norfolk, VA

Z. Ahmed*, S. Basnet, G. Huber[†], D. Paudyal, W. Li

University of Regina, Regina, SK S4S 0A2, Canada

V. Sulkosky

University of Regina, Regina, SK S4S 0A2, Canada

[†] Contact person , * Spokesperson

Contents

Abstract

We propose to measure the transverse nucleon, single-spin asymmetry $A_{UT}^{sin(\phi-\phi_s)}$ in the exclusive $\vec{n}(e, e'\pi^-)p$ reaction, during the transversely polarized ^{3}He target SIDIS experiment (i.e. E12-10-006 [1]) with SoLID [2]. This polarization observable has been noted as being sensitive to the spin-flip generalized parton distribution (GPD) $\tilde{E}$, and factorization studies have indicated that precocious scaling is likely to set in at moderate $Q^2 \sim 2 - 4$ GeV^2, as opposed to the absolute cross section, where scaling is not expected until $Q^2 > 10$ GeV^2. Furthermore, this observable has been noted as being important for the reliable extraction of the charged pion form factor from pion electroproduction. The asymmetry data are projected to be of much higher quality than a pioneering measurement by HERMES [3].

This measurement is complementary to a proposal reviewed by PAC39 [4] for the SHMS+HMS in Hall C. The asymmetry that is most sensitive to $\tilde{E}$ is the longitudinal photon, transverse nucleon, single-spin asymmetry $A_L^\perp$ in exclusive charged pion electroproduction. The SHMS+HMS allow the L–T separation needed to reliably measure this quantity. However, the limited detector acceptance and the error-magnification inherent in an L–T separation necessitates the use of a next generation, externally polarized, continuous flow, high luminosity ^{3}He target based on a large volume polarizer and compressor being developed at the University of New Hampshire.

A wide $-t$ coverage is needed to obtain a good understanding of the asymmetry. Thus, it has always been intended to complement the SHMS+HMS $A_L^\perp$ measurement with an unseparated $A_{UT}^{sin(\phi-\phi_s)}$ measurement using a large solid angle detector. The high luminosity capabilities of SoLID make it well-suited for this measurement. Since an L–T separation is not possible with SoLID, the observed asymmetry is expected to be diluted by the ratio of the longitudinal cross section to the unseparated cross section. This was also true for the pioneering HERMES measurements, which provided a valuable constraint to models for the $\tilde{E}$ GPD.

1 Scientific Justification

1.1 Generalized Parton Distributions and Contribution from the Pion Pole

In recent years, much progress has been made in the theory of generalized parton distributions (GPDs). Unifying the concepts of parton distributions and of hadronic form factors, they contain a wealth of information about how quarks and gluons make up hadrons. The key difference between the usual parton distributions and their generalized counterparts can be seen by representing them in terms of the quark and gluon wavefunctions of the hadron. While the usual parton distributions are obtained from the squared hadron wavefunction representing the probability to find a parton with specified polarization and longitudinal momentum fraction x in the fast moving hadron (Fig. 1a), GPDs represent the interference of different wavefunctions, one where the parton has momentum fraction $x + \xi$ and one where this fraction is $x - \xi$ (Fig. 1b). GPDs thus correlate different parton configurations in the hadron at the quantum mechanical level. A special kinematic regime is probed in deep exclusive meson production, where the initial hadron emits a quark-antiquark or gluon pair (Fig. 1c). This has no counterpart in the usual parton distributions and carries information about $q\bar{q}$ and gg-components in the hadron wavefunction.
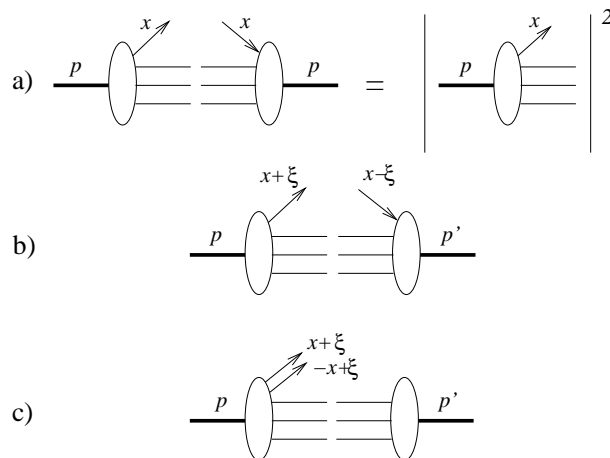

Figure 1:   (a) Usual parton distribution, representing the probability to find a parton with momentum fraction x in the nucleon. (b) GPD in the region where it represents the emission of a parton with momentum fraction $x + \xi$ and its reabsorption with momentum fraction $x - \xi$. (c) GPD in the region where it represents the emission of a quark-antiquark pair, and has no counterpart in the usual parton distributions. This figure has been adapted from Ref. [5].

Apart from the momentum fraction variables x and ξ, GPDs depend on the four momentum transfer t. This is an independent variable, because the momenta p and p' may differ in either their longitudinal or transverse components. GPDs thus interrelate the longitudinal and transverse momentum structure of partons within a fast moving hadron.

In order to access the physics contained within GPDs, one is restricted to the hard scattering regime. An important feature of hard scattering reactions is the possibility to separate clearly the perturbative and nonperturbative stages of the interaction. Qualitatively speaking, the presence of a hard probe allows one to create small size quark-antiquark and gluon configurations, whose interactions are described by perturbative

QCD (pQCD). The non-perturbative stage of the reaction describes how the hadron reacts to this configuration, or how this probe is transformed into hadrons. This separation is the so-called factorization property of hard reactions. Deep Exclusive Meson electro-Production (DEMP) was first shown to be factorizable in Ref. [6]. This factorization applies when the virtual photon is longitudinally polarized, which is more probable to produce a small size configuration compared to a transversely polarized photon.

GPDs are universal quantities and reflect the structure of the nucleon independently of the reaction which probes the nucleon. At leading twist-2 level, the nucleon structure information can be parameterized in terms of four quark chirality conserving GPDs, denoted H, E, $\tilde{H}$ and $\tilde{E}$. H and E are summed over quark helicity, while $\tilde{H}$ and $\tilde{E}$ involve the difference between left and right handed quarks. H and $\tilde{H}$ conserve the helicity of the proton, while E and $\tilde{E}$ allow for the possibility that the proton helicity is flipped. Because quark helicity is conserved in the hard scattering regime, the produced meson acts as a helicity filter. In particular, leading order QCD predicts that vector meson production is sensitive only to the unpolarized GPDs, H and E, whereas pseudoscalar meson production is sensitive only to the polarized GPDs, $\tilde{H}$ and $\tilde{E}$. In contrast, deeply virtual Compton scattering (DVCS) depends at the same time on both the polarized ($\tilde{H}$ and $\tilde{E}$) and the unpolarized (H and E) GPDs. This makes DEMP reactions complementary to the DVCS process, as it provides an additional tool to disentangle the different GPDs [7].

Besides coinciding with the parton distributions at vanishing momentum transfer ξ, the GPDs have interesting links with other nucleon structure quantities. Their first moments are related to the elastic form factors of the nucleon through model-independent sum rules [8]:

$$\sum_q e_q \int_{-1}^{+1} dx H^q(x,\xi,t) = F_1(t), \tag{1}$$

$$\sum_q e_q \int_{-1}^{+1} dx E^q(x,\xi,t) = F_2(t), \tag{2}$$

$$\sum_q e_q \int_{-1}^{+1} dx \tilde{H}^q(x,\xi,t) = G_A(t), \tag{3}$$

$$\sum_q e_q \int_{-1}^{+1} dx \tilde{E}^q(x,\xi,t) = G_P(t), \tag{4}$$

where e_q is the charge of the relevant quark, $F_1(t)$, $F_2(t)$ are the Dirac and Pauli elastic nucleon form factors, and $G_A(t)$, $G_P(t)$ are the isovector axial and pseudoscalar nucleon form factors. The t-dependence of $G_A(t)$ is poorly known, and although $G_P(t)$ is an important quantity, it remains highly uncertain because it is negligible at the momentum transfer of β-decay [9]. Because of partial conservation of the axial current (PCAC), $G_P(t)$ alone receives contributions from $J^{PG} = 0^{--}$ states [10], which are the quantum numbers of the pion, and so $\tilde{E}$ contains an important pion pole contribution (Fig. 2a).

Accordingly, Refs. [11, 12] have adopted the pion pole-dominated ansatz

$$\tilde{E}^{ud}(x,\xi,t) = F_\pi(t) \frac{\theta(\xi > |x|)}{2\xi} \phi_\pi(\frac{x+\xi}{2\xi}), \tag{5}$$

where $F_\pi(t)$ is the pion electromagnetic form factor, and ϕ_π is the pion distribution amplitude.

$\tilde{E}$ cannot be related to already known parton distributions, and so experimental information about $\tilde{E}$ via DEMP can provide new information on nucleon structure which is unlikely to be available from any other source.
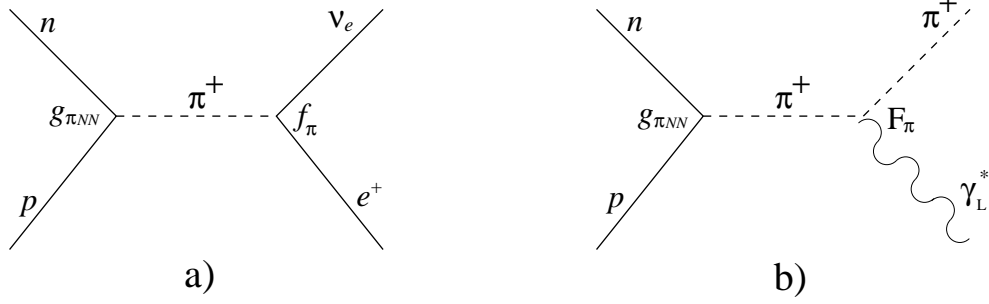
Figure 2: (a) Pion pole contribution to $G_P(t)$, and hence to $\tilde{E}$. (b) Pion pole contribution to meson electroproduction at low $-t$.
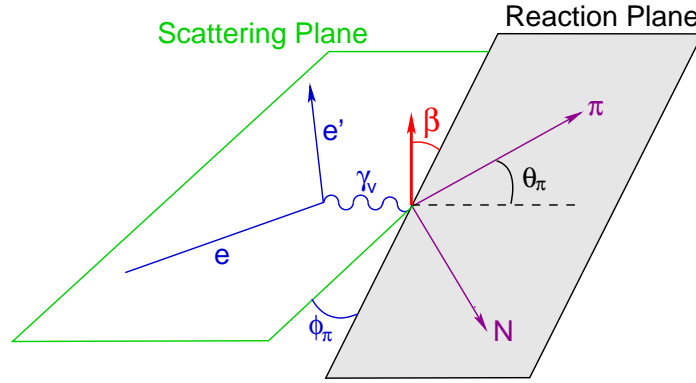

Figure 3: Scattering and hadronic reaction planes for exclusive $\vec{N}(e, e'\pi)N'$. β is the angle between the target nucleon polarization vector and the reaction plane. Some works alternatively label this angle as $(\phi - \phi_s)$.

1.2 Single spin asymmetry in exclusive pion electroproduction

Frankfurt et al. [13] have considered a specific polarization observable which is the most sensitive observable to probe the spin-flip $\tilde{E}$. This variable is the single-spin asymmetry for exclusive charged pion production, $\vec{p}(e, e'\pi^+)n$ or $\vec{n}(e, e'\pi^-)p$, from a transversely polarized nucleon target, and is defined [12] as

$$A_L^\perp = (\int_0^\pi d\beta \frac{d\sigma_L^\pi}{d\beta} - \int_\pi^{2\pi} d\beta \frac{d\sigma_L^\pi}{d\beta})(\int_0^{2\pi} d\beta \frac{d\sigma_L^\pi}{d\beta})^{-1}, \tag{6}$$

where $d\sigma_L^\pi$ is the exclusive charged pion electroproduction cross section using longitudinally polarized photons and β is the angle between the nucleon polarization vector and the reaction plane (Fig. 3). Frankfurt et al. [13] have shown that this asymmetry must vanish if $\tilde{E}$ is zero. If $\tilde{E}$ is not zero, the asymmetry will display a $\sin\beta$ dependence. Their predicted asymmetry using the $\tilde{E}$ ansatz from Ref. [14] is shown in Fig. 4. This calculation is Q^2-independent, depending only on how well the soft contributions cancel in the asymmetry.

It seems likely that a precocious factorization of the meson production amplitude into three parts – the overlap integral between the photon and pion wave functions, the hard interaction, and the GPD – will lead to a precocious scaling of $A_L^\perp$ as a function of Q^2 at moderate $Q^2 \sim 2-4$ GeV^2 [13]. This precocious scaling arises from the fact that higher order corrections, which are expected to be significant at low Q^2, will likely
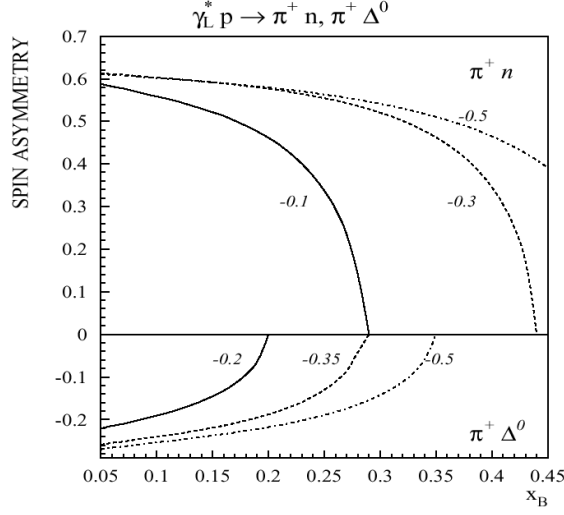
Figure 4: Transverse single-spin asymmetry for the longitudinal electroproduction of $\pi^+ n$ and $\pi^+ \Delta^0$ at different values of t [indicated on the curves in GeV^2]. The asymmetry drops to zero at the parallel kinematic limit, which is different for each t value, because the definition of β is ill-defined at this point. This figure is taken from Ref. [15].

cancel when one examines the ratio of two longitudinal observables. In contrast, the onset of scaling for the absolute cross section is only expected for much larger values of $Q^2 > 10$ GeV^2.

This point is made clear in Fig. 5. This figure shows renormalon model calculations [16] of both the asymmetry and the longitudinal cross section at $Q^2 = 4$ GeV^2. While the magnitude of the cross section changes significantly when taking into account the twist-four corrections, $A_L^\perp$ is essentially insensitive to them and displays the expected precocious scaling. The relatively low value of Q^2 for the expected onset of precocious scaling is important, because it will be experimentally accessible after the Jefferson Lab 12 GeV upgrade. This places $A_L^\perp$ among the most important GPD measurements that can be made in the meson scalar. If precocious scaling cannot be experimentally demonstrated in this ratio of two cross sections, then it may not be possible to determine GPDs from DEMP data.

Refs. [7] and [15] also point out that the study of the transverse target single-spin asymmetry versus t is important for the reliable extraction of the pion form factor from electroproduction experiments (Fig. 2b). Investigations of hard exclusive π^+ electroproduction using a pQCD factorization model [17, 18] find that at $x_B = 0.3$ and $-t = -t_{min}$, the pion pole contributes about 80% of the longitudinal cross section. Since the longitudinal photon transverse single-spin asymmetry is an interference between pseudoscalar and pseudovector contributions, its measurement would help constrain the non-pole pseudovector contribution, and so assist the more reliable extraction of the pion form factor. The upper $Q^2 = 6$ GeV^2 limit of the approved pion form factor measurements in the JLab 12 GeV program [19] is dictated primarily by the requirement $-t_{min} < 0.2$ GeV^2, to keep non-pion pole contributions to σ_L at an acceptable level [18]. Transverse target single-spin asymmetry studies versus t may eventually allow, with theoretical input, the use of somewhat larger $-t$ data for pion form factor measurements, ultimately extending the Q^2-reach of pion form factor data acquired with JLab 12 GeV beam. Thus, measurements of the transverse single-spin
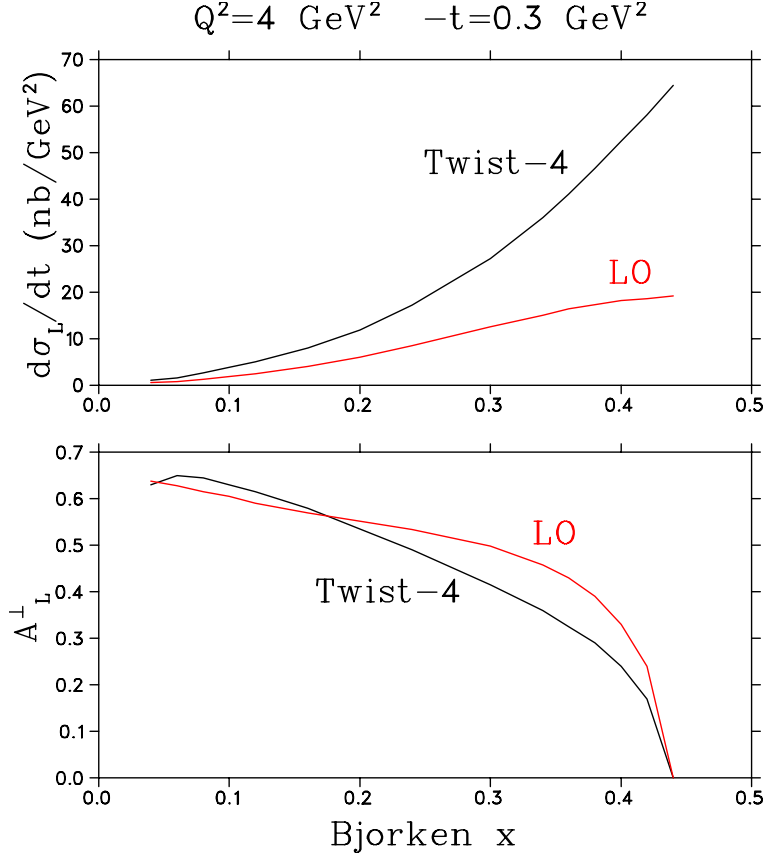
Figure 5: Calculation of the longitudinal photon transverse nucleon spin asymmetry including twist-four corrections by A. Belitsky [16] at $-t = 0.3$ GeV^2, Q^2=4 GeV^2. The red curves are the leading order calculation, while the black curves have twist-four power effects taken into account. While the cross section is very sensitive to these corrections, the transverse spin asymmetry is stable.

asymmetry are a logical step in the support of the pion form factor program.

1.3   The Complementarity of Separated and Unseparated Asymmetry Measurements

The reaction of interest is $^3He(e, e'\pi^-)p(pp)_{sp}$. The measurement of the transverse single-spin asymmetry requires the detection of the π^- in non-parallel kinematics. It is the component of the target polarization parallel to $\hat{q} \times \hat{p_\pi}$ that is important, and this direction is uniquely defined only in non-parallel kinematics.

Experimentally, the angle between the target polarization and the reaction plane, β, and the angle between the scattering and reaction planes, ϕ, are not independent. If the target polarization is at some angle, ϕ_s, relative to the scattering plane, then $\beta = \phi_s - \phi$. The polarized nucleon cross section can be

expressed [20] in terms of these variables as:

$$\sigma_t = -P_\perp \sin\beta \left[\sigma_{TT}^y + 2\epsilon\,\sigma_L^y\right]$$

$$- P_\perp \sin\beta \left[\epsilon(\cos 2\phi_s \cos 2\beta + \sin 2\phi_s \sin 2\beta)\,\sigma_{TT'}^y\right]$$

$$- P_\perp \sin\beta \left[\sqrt{2\epsilon(1+\epsilon)}(\cos\phi_s \cos\beta + \sin\phi_s \sin\beta)\,\sigma_{LT}^y\right]$$

$$- P_\perp \cos\beta \left[\sqrt{2\epsilon(1+\epsilon)}(\sin\phi_s \sin\beta - \cos\phi_s \cos\beta)\,\sigma_{LT}^x\right]$$

$$- P_\perp \cos\beta \left[\epsilon(\sin 2\phi_s \sin 2\beta - \cos 2\phi_s \cos 2\beta)\,\sigma_{TT}^x\right]. \quad (7)$$

From the above equation, it is clear that to extract $A_L^\perp$ it is necessary to first isolate the $\sin\beta$ Fourier component of the polarized nucleon cross section. Once that has been accomplished, one must then separate the σ_L^y term from the σ_{TT}^y term via a Rosenbluth-type separation.

It has not yet been possible to perform an experiment to measure $A_L^\perp$. The conflicting experimental requirements of transversely polarized target, high luminosity, L–T separation, and closely controlled systematic uncertainty, make this an exceptionally challenging observable to measure. The SHMS+HMS is the only facility with the necessary resolution and systematic error control to allow a measurement of $A_L^\perp$. However, the beamtime required to do a good measurement with current polarized target technology is in the range of 10^3 days. To minimize the beamtime required, PR12-12-005 [4] proposed the use of a next generation, externally polarized, continuous flow, high luminosity ^{3}He target based on a large volume polarizer and compressor developed at the University of New Hampshire. The science case for this measurement was favorably reviewed by PAC39, and they encouraged the continued development of the target technology. Although the New Hampshire group is making continued progress on the development of the target, there is no timeline for its actual implementation at Jefferson Lab.

The most closely related measurement, of the transverse single-spin asymmetry in exclusive π^+ electroproduction without an L–T separation, was published by the HERMES Collaboration in 2010 [3]. Their data were obtained for average values of $\langle x_B \rangle = 0.13$, $\langle Q^2 \rangle = 2.38$ GeV^2 and $\langle t' \rangle = -0.46$ GeV^2, subject to the criterion $W^2 > 10$ GeV^2. The six Fourier amplitudes in terms of the azimuthal angles ϕ, ϕ_s of the pion-momentum and proton-polarization vectors relative to the lepton scattering plane were determined. Of these, at leading twist only the $\sin(\phi - \phi_s)_{UT}$ Fourier amplitude receives a contribution from longitudinal photons. If one assumes that longitudinal contributions dominate, these $A_{UT}^{\sin(\phi-\phi_s)}$ values can be compared to GPD models for $\tilde{E}$, $\tilde{H}$.

Because transverse photon amplitudes are suppressed by $1/Q$, at very high Q^2 it is safe to assume that all observed meson production is due to longitudinal photons. At the lower Q^2 typical of the JLab and HERMES programs, however, this is not the case. Calculations by Goloskokov and Kroll [21] indicate much of the unseparated cross section measured by HERMES [3] is due to contributions from transversely polarized photons. In addition, there are contributions to $A_{UT}^{\sin(\phi-\phi_s)}$ from the interference between two amplitudes, both for longitudinal photons, as well as transverse photons [22]. As indicated in Fig. 6, the contribution from transverse photons tends to make the asymmetry smaller. At the HERMES kinematics, the dilution caused by transverse photons is about 50%.

A run-group proposal concurrent with the SoLID transversely polarized ^{3}He SIDIS experiment allows for an unseparated asymmetry measurement to be obtained on a sooner timescale than the Hall C measurement. In comparison to the HERMES measurement, the experiment proposed here will probe higher Q^2 and x_B,
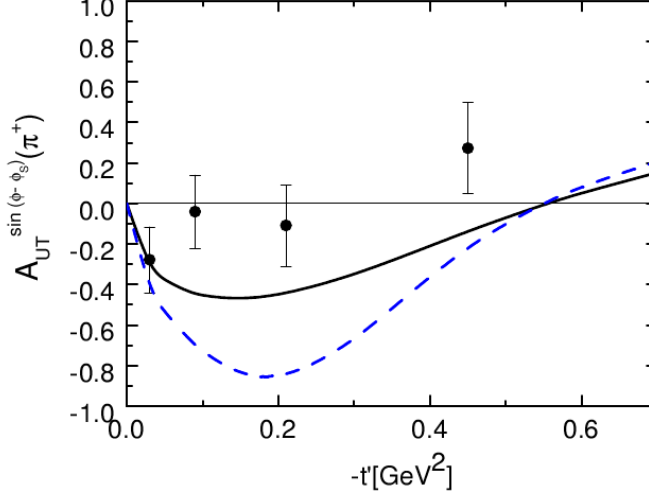
Figure 6: Predictions by Goloskokov and Kroll for the $\sin(\phi - \phi_s)$ moment of A_{UT} in the handbag approach, in comparison to the data from HERMES at $Q^2 = 2.45$ GeV^2, $W = 3.99$ GeV. The independent variable is $-t' = |t - t_{min}|$. Dashed line: contribution from longitudinal photons only. Solid line: full calculation including both transverse and longitudinal photons. This figure is taken from Ref. [21].

with much smaller statistical errors over a wider range of $-t$. SoLID will allow the first measurement for $Q^2 > 4$ GeV^2, where GPD-based calculations are expected to apply. Thus, the measurements should be more readily interpretable than those from HERMES. Similar measurements using CLAS-12 and a transversely polarized ^{1}H target have been discussed previously [23], but this measurement will allow for smaller statistical uncertainties, due to SoLID's higher luminosity capabilities.

Handbag model calculations by Goloskokov and Kroll [24] shed further light on the expected asymmetry dilution. The lower left panel of Fig. 7 shows their predictions for the cross section components in exclusive charged pion production. Although their calculations tend to underestimate the σ_L values measured in the JLab $F_\pi - 2$ experiment [25], their model is in reasonable agreement with the unseparated cross sections [21]. They predict significant transverse contributions for JLab kinematics. A comparison of the unseparated asymmetry at $-t = 0.3$ GeV^2, $x_B = 0.365$ in Fig. 7 with the separated longitudinal asymmetry at the same values of x_B, $-t$ in Fig. 5 indicates a substantial dilution of the unseparated asymmetry due to transverse photon contributions, similar to that observed in Fig. 6.

In addition to allowing a measurement at $Q^2 > 4$ GeV^2, a measurement by SoLID of $A_{UT}^{sin(\phi-\phi_s)}$ will cover a fairly large range of $-t$, allowing the asymmetry to be mapped over its full range with good statistical uncertainties – from its required zero-value in parallel kinematics, through its maximum, and then back to near-zero as σ_T dominates σ_L at larger $-t$. The shape of the asymmetry curve versus $-t$, as well as its maximum value, are critical information for comparison to GPD-based models. At a later date, the New Hampshire polarized target might enable a measurement of $A_L^\perp$ in Hall C. The comparison of the maxima and t-dependences of both measurements will provide complementary data needed to extract $\tilde{E}$ information and better understand non-pole contributions complicating the extraction of the pion form factor from electroproduction data.
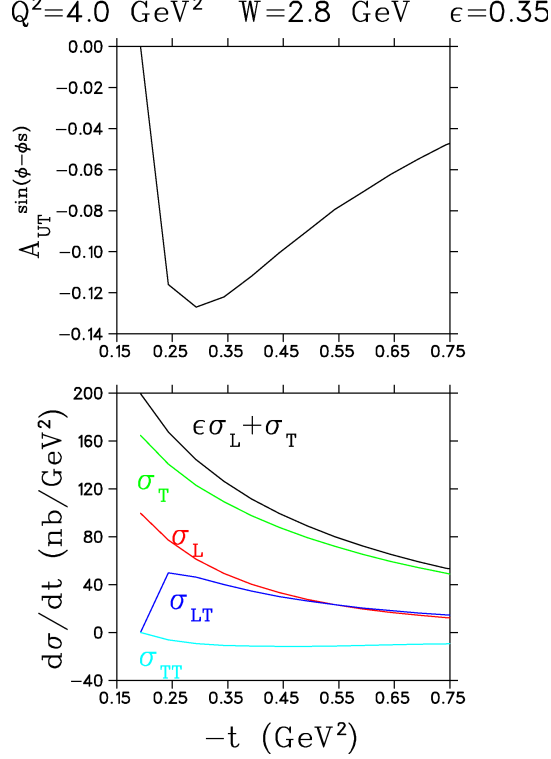
Figure 7: Calculation of the cross section components and $\sin(\phi - \phi_s)$ moment of the transverse nucleon spin asymmetry A_{UT} in the handbag approach by Goloskokov and Kroll [24] for kinematics similar to those in Fig. 5. Our measurement will be at higher $0.55 < \epsilon < 0.75$ than the $\epsilon = 0.35$ kinematics of this figure, so the dilution in the asymmetry will be significantly less.

2 Experimental Method

We propose to carry out the $^3He(e, e'\pi^-)p(pp)_{sp}$ measurement using the Solenoidal Large Intensity Device (SoLID [2]), in parallel with the already approved experiment, E12-10-006 [1], which will measure Semi-Inclusive Deep-Inelastic Scattering (SIDIS). Our discussion will concentrate on the region of clearest physics interpretation ($Q^2 > 4$ GeV^2), even through lower Q^2 events will also be contained in the experimental data-set.

There are two SoLID configurations, called SoLID-SIDIS and SoLID-PVDIS. Besides E12-10-006, two SIDIS experiments, E12-11-007 [26] and E12-11-108 [27], along with the J/ψ experiment (E12-12-006 [28]), will use the SoLID-SIDIS configuration as well. All of these experiments have been approved with A or A-rating. In addition, two "bonus-run" experiments, E12-10-006A [29] and E12-11-108A [30], have also been approved to run in parallel with the SIDIS experiments. The SoLID-PVDIS configuration is for the Parity Violation in Deep Inelastic Scattering (PVDIS).

The experiment will use a near identical setup as E12-10-006, but with few additions without affecting the approved experiment. We will use exactly the same online production trigger, which is the coincidence of electron triggers and hadron triggers. We will perform the offline analysis to identify the protons from DEMP and form the triple coincidence events together with electrons and π^- provided by SIDIS triggers.

The SoLID-SIDIS detector can only detect protons with scattering angles from $8°$ up to $24°$, while the main proton events from the DEMP process can cover $0°$ up to $50°$. We propose to add a new proton recoil detector (PRD) based on scintillator counters to detect protons with angles from $24°$ to $50°$. The new detector will be placed between the target system and the entrance of the solenoid magnet. The proton identification and the conceptual design of the new proton detector will be discussed in more detail in the following sections and in Appendix-B.

2.1 Transversely Polarized ^{3}He Target

Target	^{3}He
Length	40 cm
Target Polarization	$\sim 60\%$
Target Spin Flip	≤ 20 mins
Target Dilution	90%
Effective Neutron	86.5%
Target Polarimetry Accuracy	$\sim 3\%$

Table 1: Key Parameters of the ^{3}He target.

The proposed measurement will utilize the same polarized ^{3}He target as E12-10-006 [1]. Such a target was successfully employed in E06-110, a 6 GeV SIDIS experiment in Hall A. A wide range of experiments have utilized polarized ^{3}He as an effective neutron target over a wide range of kinematics. And over the past decades several authors have calculated the effective neutron polarization in ^{3}He using three-nucleon wave functions and various models of the $N - N$ interaction [32]. These are now well established, and the error introduced by uncertainty in the wave functions are small.

Other nuclear effects which can influence the experimental asymmetry for a neutron bound inside ^{3}He include Fermi motion, off-shell effects, meson exchange currents, delta isobar contributions and π^- final state interactions. The exclusive nature of the process, the selected kinematics such as high Q^2, large recoil momentum and a complete coverage of the azimuthal angle ϕ ensures that corrections due to these nuclear effects will be small and can be modeled effectively.

The ^{3}He polarization direction is held by three sets of Helmholtz coils with a 25 Gauss magnetic field. Both the transverse and longitudinal directions can be provided by rotating the magnetic field. The ^{3}He gas, with density of about 10 atm (at $0°$ C), is stored in a 40 cm target cell made of thin glasses. With a 15 μA electron beam, the neutron luminosity can be as high as $10^{36} \text{cm}^{-2}\text{s}^{-1}$. In-beam polarization of 60% was archived during the E06-110 experiment. Two kinds of polarimetry, NMR and EPR, were used to measure the polarization with relative 5% precision. We have plans to improve the accuracy of the measurement to reach 3%.

The target spin will be reversed for every 20 minutes by using the RF AFP technique. The additional polarization loss due to the spin reversal was kept at < 10 %, which has been taken into account in the overall 60% in-beam polarization. A new method for spin reversal using field rotation has been tested and was able to eliminate the polarization loss. Such an improvement will enable us to perform the spin-reversal in few minutes to reduce the target-spin-correlated systematic errors. The key parameters of the ^{3}He target

are summarized in Table 1.

A collimator, similar to the one used in the E06-110, will be placed next to the target cell window to minimize the target cell contamination and to reduce the event rate. Several calibration targets will also be installed in this target system, including a multi-foil ^{12}C for optics study, a BeO target for beam tuning, and a reference target cell for dilution study and other calibration purposes.

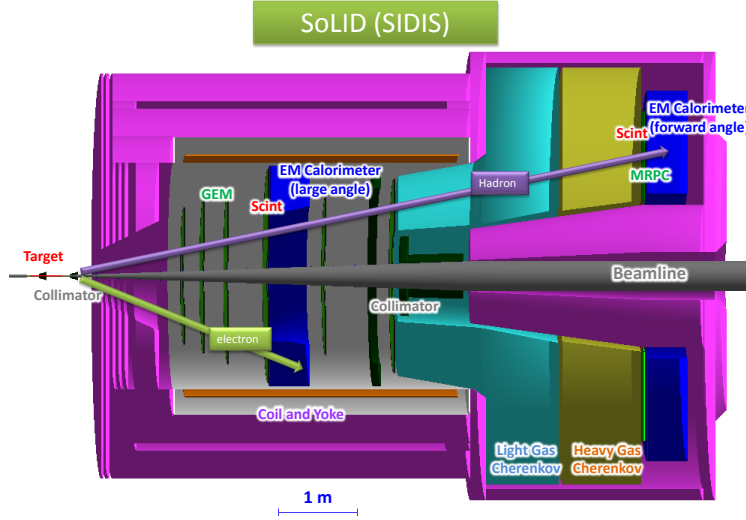## 2.2 SoLID Spectrometer and Detectors

Figure 8: The Detector Layout of the SoLID-SIDIS configuration. The detector system includes six Gas Electron Multiplier (GEM) planes for charged particle tracking, two Scintillator Pad Detectors (SPD) followed by two Shashlyk sampling EM Calorimeters (EC) for energy measurement and particle identification, a Light Gas Čerenkov Detector (LGC) for e-$\pi^{\pm}$ separation, a Heavy Gas Čerenkov Detector (HGC) for $\pi^{\pm}$-$K^{\pm}$ separation, as well as a Multi-gap Resistive Plate Chamber (MRPC) for timing measurement. The first four GEM trackers, the first SPD (i.e. LASPD) and EC (i.e. LAEC) form the large-angle detection system for electron measurement. The forward-angle detection system, to measure electron and hadrons, is composed of all six GEM trackers, LGC, HGC, MRPC, the second SPD (i.e. FASPD) and the second EC (FAEC).

The solenoid magnet for SoLID will be based on the CLEO-II magnet built by Cornell University. The magnet is 3 meters long with an outer diameter of 3 meters and an inner diameter of 1 meter. The field strength is greater than 1.35 Tesla, with an integrated BDL of 5 Tesla-meters. The fringe field at the front end after shielding is less than 5 Gauss. In the SIDIS-configuration, the CLEO-II magnet provides 2π acceptance in the azimuthal angle (ϕ) and covers polar angle (θ) from 8° up to 24°. The momentum acceptance is between 0.8 and 7.5 GeV/c for electrons and for hadrons, the momentum can be lower depending on the trigger efficiency. The momentum resolution is about 2%.

The layout of the SoLID detectors in the SIDIS-configuration is shown in Fig. 8. The detector system is divided into two regions for the forward-angle (FA) detection and the large-angle (LA) detection. Six tracking chambers based on Gas Electron Multipliers (GEM) will be used for charged particle tracking in the forward-angle region, and the first four of them will be shared by the large-angle region. In each region, a Shashlyk-type sampling EM calorimeter (LAEC or FAEC) will measure the particle energy and

13

Experiments	SIDIS	DEMP
Reaction channel	$\vec{n}(e,e'\pi^{\pm})X$	$\vec{n}(e,e'\pi^{-}p)$
Target	^{3}He	same
Unpolarized luminosity	$\sim 10^{37}$ cm^{-2}s^{-1} per nucleon	same
Momentum coverage	0.8-7.5 (GeV/c) for $e^{-},\pi^{\pm}$	same
		0.3 1.2 (GeV/c) for protons
Momentum resolution	$\sim$2%	same
Azimuthal angle coverage	0° 360°	same
Azimuthal angle resolution	5 mr	same
Polar angle coverage	8°-24° for e	same
	8°-14.8° for $\pi^{\pm}$	same
		8°-24 ° for p
		24°-50° for p with recoil detector
Polar angle resolution	0.6 mr	same
Target Vertex resolution	0.5 cm	same
Energy resolution on ECs	5%$\sim$10%	same
Trigger type	Double Coincidence $e^{-} + \pi^{\pm}$	same (online)
		Triple Coincidence $e^{-} + \pi^{-} + p$ (offline)
Expected DAQ rates	<100 kHz	same (online)
Main Backgrounds	^{3}He(e,e'K$^{\pm}$/π^{0})X	^{3}He(e,e'$\pi^{\pm}$/K$^{\pm}$)X
	Accidental Coincidence	Accidental Coincidence
Key requirements	Radiation hardness	Proton Detection
	Kaon Rejection	Exclusivity
	DAQ	Timing Resolution

Table 2: Summary of Key Parameters for DEMP Measurement compared with SIDIS Experiments.

identify electrons from hadrons. A scintillator-pad detector (LASPD and FASPD) will be installed in front of each EC to reject photons and provide timing information. The forward-angle detectors will detect both the electrons and hadrons (mainly $\pi^{\pm}$). A light-gas Čerenkov detector (LGC) and a heavy-gas Čerenkov detector (HGC) will perform the $e/\pi^{\pm}$ and $\pi^{\pm}/K^{\pm}$ separation, respectively. The Multi-gas Resistive Plate Chamber (MRPC) will provide a precise timing measurement and serve as a backup of the FASPD on photon rejection. A more detailed discussion of the design, simulation, prototype-test of each detector is given in the SoLID preliminary conceptual design report (pCDR) [2].

Table 2 summarizes the key parameters of the detector system in the SIDIS configuration for both the SIDIS and DEMP measurements.

2.3 Proton Identification

The cleanest way to identify the DEMP events is to detect all particles in the final state. The SoLID-SIDIS detector system has the capability of measuring electrons and pions, while protons can be isolated from other charged particles by using the time-of-flight (TOF) information. The TOF is provided by the timing
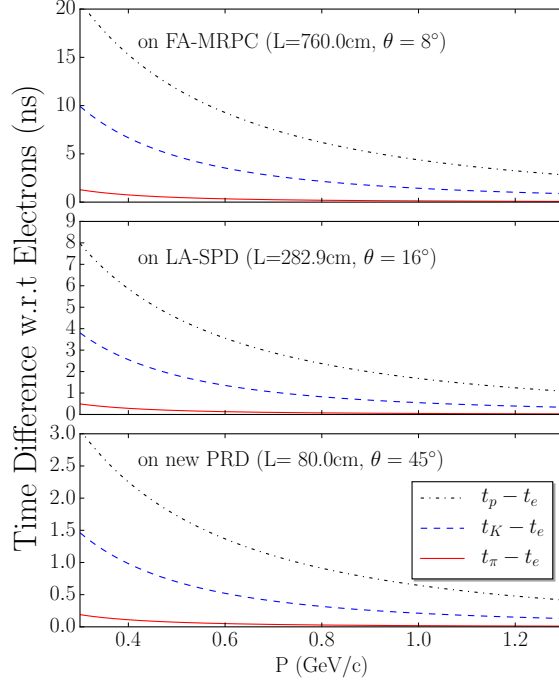
Figure 9: The time differences (in ns) between electrons and other charged particles, i.e. pions (red solid line), kaons (blue dashed line) and proton (black dash-dotted line), and their distributions as functions of particles' momentum at three different timing detectors, including the forward-angle (FA) MRPC, the large-angle (LA) SPD, and the potential new proton recoil detector discussed in Appendix-B.

detectors, including the MRPC and FASPD at the forward-angle detection region, the LASPD at the large-angle detection region and the proposed new PRD near the target. A discussion of the potential new proton recoil detector and its conceptual design is given in Appendix-B. In this proposal, we present projections for two scenarios: (a) triple coincidence $e - \pi^- - p$ in SoLID only, (b) the improved data that can be acquired if the PRD is constructed.

We examined the requirement of the timing resolution on these detectors by looking at the time difference between electrons and other heavier charged particles when they reach these detectors with the same momentum and flight path. To be shown in the next section, the good protons from the DEMP reaction carry momenta from 0.3 GeV/c up to 1.2 GeV/c with angles from 0° to 50°. The FA-MRPC covers angles from 8° to 14.8°, the angular range of the LASPD is from 16° to 24°, and we expect to use the new PRD to detect protons with angles larger than 24°. Hence we simulated events of electrons, pions, kaons and protons with the momentum from 0.3 GeV/c up to 1.2 GeV/c, and calculated the time when they reach three detectors with linear trajectories and at fixed angles.

The results are shown in Fig. 9. To clearly identify two types of charged particles with the same momentum, we normally require the timing difference between two particles to be larger than 5 times of the overall timing resolution, while the SoLID timing detectors can reach the resolution in the range of 150 ps down to 50 ps. At the FA-MRPC, which is more than 7 meters from the target, protons come 3 ns later than kaons, even at the highest momenta in the DEMP reaction. Hence, protons will be easily distinguished from other lighter particles. At the LA-SPD, which is about 3 meters away from the target, the time difference between

protons and kaons is still more than 1 ns, which doesn't demand precise timing resolution.

The new PRD has to be placed closely to the target and the TOF distance is expected to be about 80 cm. Since no momentum information is provided in this detector region, one can only rely on the one-dimensional distribution of the time-difference to identify different particles. There are more than 0.5 ns time difference between the fastest protons and the slowest electrons, and hence most of low energy electrons from Moller scattering and other processes can be suppressed when the timing resolution is better than 100 ps. The time difference between the fastest proton and the slowest pions is about 0.3 ns which may requires a timing resolution of the PRD to be better than 60 ps. However, such a requirement is currently achievable, and the SoLID collaboration is working on improving the resolution of the timing detectors to be better than 20 ps. We may not be able to cleanly separate all kaons and protons, but the event rates of kaons would be small.

In general, the misidentified events can be mostly removed by cutting on the reconstructed missing quantities, e.g. angles, momenta and masses. The residual background will also be largely suppressed in the target-spin asymmetry extraction.

2.4 Trigger Design

In E12-10-006, the online production trigger will be the double-coincidence of the scattered electrons and hadrons. One will use the particle identification detectors, such as LGC, HGC and ECs, during the offline analysis to select $\pi^{\pm}$ out from other hadrons. The DEMP events will be identified with the triple-coincidence of the scattered electron, π^- and proton, while the proton identification has been discussed above. We will use the same online trigger as the SIDIS one, and hence the new experiment will share the same data-set as E12-10-006. The actual design of the SIDIS triggers will be far more complicated, and the detailed discussion of the trigger and DAQ designs is given in the SoLID pCDR [2].

If we install a new PRD near the target area, signals from this detector will be merged into the data stream. It will increase the DAQ load and the data size, and hence it may potentially impact the SIDIS experiment. As discussed in the next section, even without the PRD, we should be able to do a good measurement and obtain much more precise TSA data at $Q^2 >4$ GeV^2 than was obtained by HERMES. Moreover, with the PRD to detect large angle protons, we can extend the $-t$ coverage from 0.6 GeV^2 to 1 GeV^2 and also largely improve the uncertainties of the asymmetries. When we design and optimize the PRD, we will take these aspects into account, and minimize the impact to the SIDIS experiments while maximizing the physics output of our measurement.

3   Projected Results

3.1   Kinematic Coverage

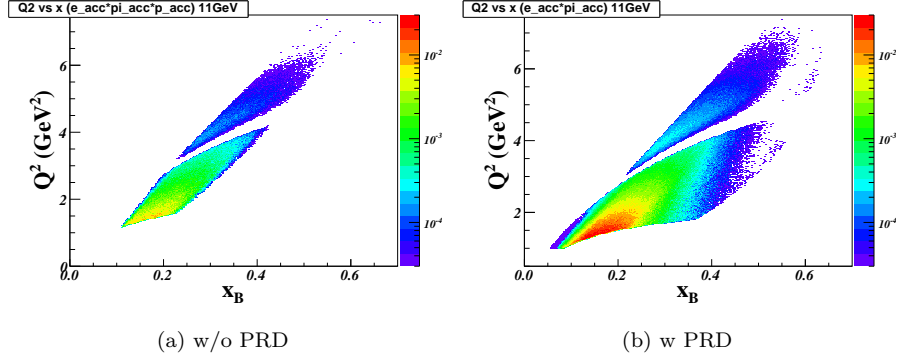(a) w/o PRD   (b) w PRD

Figure 10: The kinematic coverage at different acceptances at 11 GeV. The left plot shows the coverage with proton detection by existing SoLID detectors, while the right plot shows the coverage when detecting all recoil protons with an additional proton detector. Colors correspond to rates (Hz) in log scale.

The kinematic coverage in Q^2 vs. x_B is shown in Fig. 10, where two proton detection cases were given: (a) by using only the SoLID detectors to detect protons at small angles ($8° \sim 24°$) and adding a new proton recoil detector to detect the rest of the recoil protons at larger angle ($24° \sim 50°$), or (b) by only using only the SoLID detectors. These distributions were weighted by the DEMP unpolarized cross sections and the SoLID acceptance obtained from the GEANT4 simulation with the SoLID-SIDIS configuration. As shown in these plots, the range of Q^2 is from 1.0 GeV^2 to 8.0 GeV^2, x_B goes from 0.1 up to 0.75.

Fig. 11 shows the momentum and angular acceptance of electrons, π^- and protons which form the DEMP events and can be detected with the SoLID detectors and (or) with the new PRD. A cut of $Q^2 >4$ GeV^2 is applied since this is the region of greatest physics itnerest. The recoil protons shown in Fig. 11 have low momenta ranging from 0.3 GeV/c up to 1.2 GeV/c and their rates are distributed nearly uniformly in scattering angle.

3.2   Estimated Rates

$1< Q^2 <4$ GeV^2	$Q^2 >4$ GeV^2	Total
DEMP: $\vec{n}(e, e'\pi^- p)$ Triple-Coincidence (Hz)		
23.91 (6.21)	0.59 (0.28)	24.50 (6.49)
SIDIS: $\vec{n}(e, e'\pi^-)X$ Double-Coincidence (Hz)		
1388.85	35.77	1424.62

Table 3: Triple-Coincidence rates for DEMP events compared with the SIDIS rates. Numbers in brackets are the DEMP rates with only detecting protons using only the SoLID detectors. The online production trigger will be the SIDIS double-coincidence trigger of which rates are also given.

Table 3 lists the triple-coincidence rate of the DEMP events. The rates were calculated with the simulated
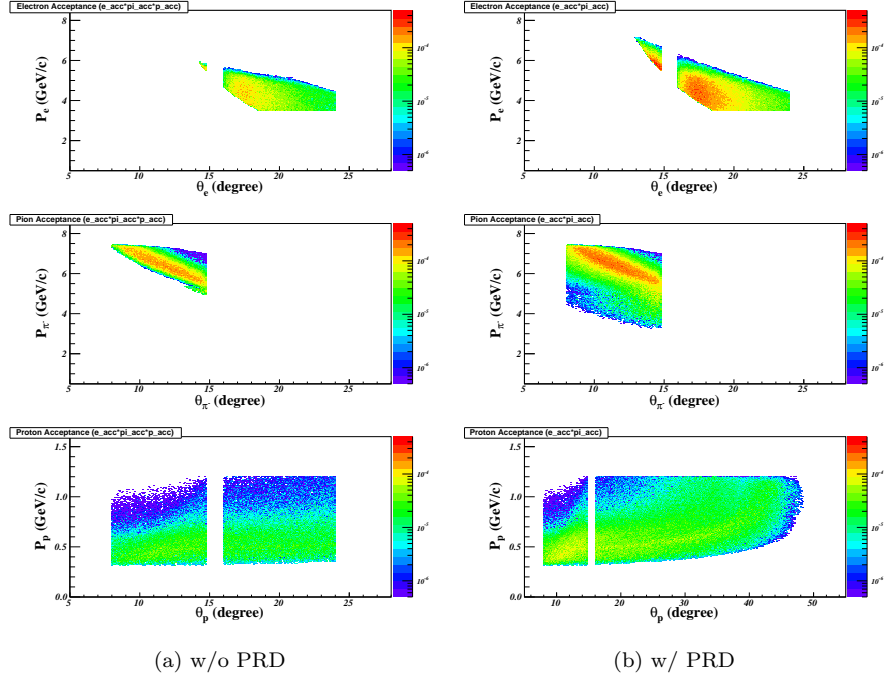
Figure 11: The acceptance of the momenta and polar angles w/o or w/ the PRD. In each panel, the top, middle and bottom plots are for electrons, π^- and protons, respectively. A cut of $Q^2 > 4$ GeV^2 is applied. Colors correspond to rates (Hz) in log scale.

events weighted by the target luminosity, the SoLID acceptances and unpolarized cross sections. The rates are not corrected by the beam and target polarization, target dilution and so on. The total integrated physics rate is estimated to be around 25 Hz at 11 GeV, or 0.59 Hz at $Q^2 > 4$ GeV^2. If only using only the SoLID detectors to detect protons, the rate drops to 0.28 Hz at $Q^2 > 4$ GeV^2. For comparison, the table also gives the SIDIS rate which will be the online production trigger rates and is the main background of the DEMP events.

3.3 Asymmetry Projections

The proposed experiment will run in parallel with E12-10-006 which has already been approved to run 48 days at E_0=11 GeV. As shown in Fig. 12, We defined 7 $-t$ bins of which the the boundaries are defined by the array:

$$-t[8] = [0.0, 0.15, 0.25, 0.35, 0.45, 0.55, 0.75, 1.10] \quad (in \text{ GeV}^2) \tag{8}$$

The number of events (N_i) in the ith bin is calculated from the total simulated events after applying cuts on important kinematic variables, e.g. $Q^2 > 4$ GeV^2, $W > 2$ GeV, $0.55 < \epsilon < 0.75$ and $-t_{min} < -t < -t_{max}$. As shown in Eq. 9, each event surviving the cuts is then weighted by the unpolarized cross section, together with the acceptance of the electron, pion and proton. N_i is further corrected by the phase-space factor (PSF) defined in the event generator, the total number of randomly generated events (N_{gen}), beam-time (T), the
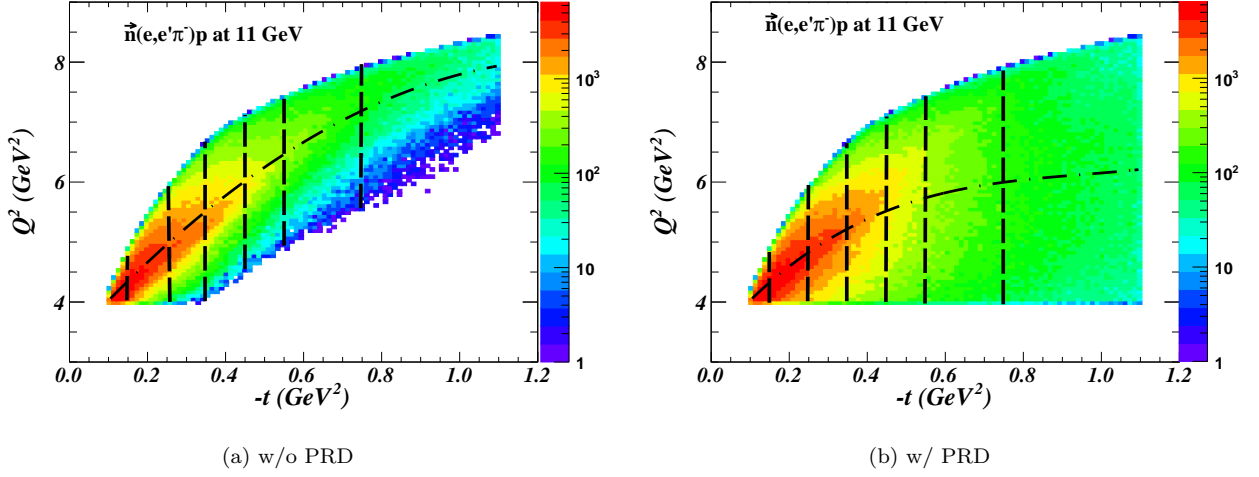
18

Figure 12: Q^2 vs. $-t$ where the black dash lines specify the boundaries of $7 -t$ bins and the black dash-dot lines indicate the additional 2 Q^2 bins. The color panel indicates the raw counts with 48 days of beam time at 11 GeV.

target luminosity ($L = 10^{36}$ cm^{-2}s^{-1}), and the overall detector efficiency (ϵ_{eff}):

$$N_i = \Big(\sum_{j \in i-bin} \sigma_j \cdot A_j^e \cdot A_j^{\pi^-} \cdot A_j^p \Big) \cdot (PSF/N_{gen}) \cdot T \cdot L \cdot \epsilon_{eff}, \tag{9}$$

where j is the jth event in the ith bin, σ_j is the cross section of the jth event. $A_j^{e(\pi^-, p)}$ is the acceptance weight of the electron (pion, proton) in this event. The detector efficiency, ϵ_{eff}, is approximately fixed at 85% which was used in SIDIS proposals. N_i corresponds to the raw experimental count of electrons scattering on neutrons in ^{3}He before taking into account the target polarization ($P \sim 60\%$), the effective polarization of neutrons ($\eta_n \sim 0.865$), and the dilution effect from other reaction channels when electrons scattering on ^{3}He ($f \sim 0.9$).

In addition, we further divide each $-t$-bin into two Q^2 bins with similar statistics. By doing that we are able to examine the Q^2-dependence of the asymmetries, and also check the model dependence of other corrections that are directly related to the values of Q^2.

The statistical error of the target single spin asymmetry (A_{UT}) in each bin can be given as:

$$\delta A_{UT} = \frac{1}{P \cdot \eta_n \cdot f} \sqrt{\frac{1 - (P \cdot <A_{UT}>)^2}{N_i^+ + N_i^-}}, \tag{10}$$

where $N_i^{+(-)}$ is the number of counts in each bin when the target polarization is up (down), and we easily have $N_i = N_i^+ + N_i^-$; $<A_{UT}>$ is the average asymmetry in the bin, and experimentally, it can be extracted as following:

$$<A_{UT}> = \frac{1}{P \cdot \eta_n \cdot f} \frac{N^+ - N^-}{N^+ + N^-}. \tag{11}$$

In this projection study, A_{UT} is predicted with a phenomenological model, as discussed in Appendix-A. Because of not performing a L/T separation in this experiment, the asymmetry should be corrected by another dilution factor which is defined as:

$$f_{L/T} = \frac{\epsilon \sigma_L}{\sigma_T + \epsilon \cdot \sigma_L}, \tag{12}$$

19

where $\epsilon = (1 + \frac{2\nu^2}{Q^2}\tan^2(\theta))^{-1}$. Additional dilution due to σ_{TT} is assumed to be small. A factor of -1 is also applied after comparing Eq. 6 and Eq. 7. Hence, $A_{UT} = -f_{L/T} \cdot A_L^{\perp,model}$.
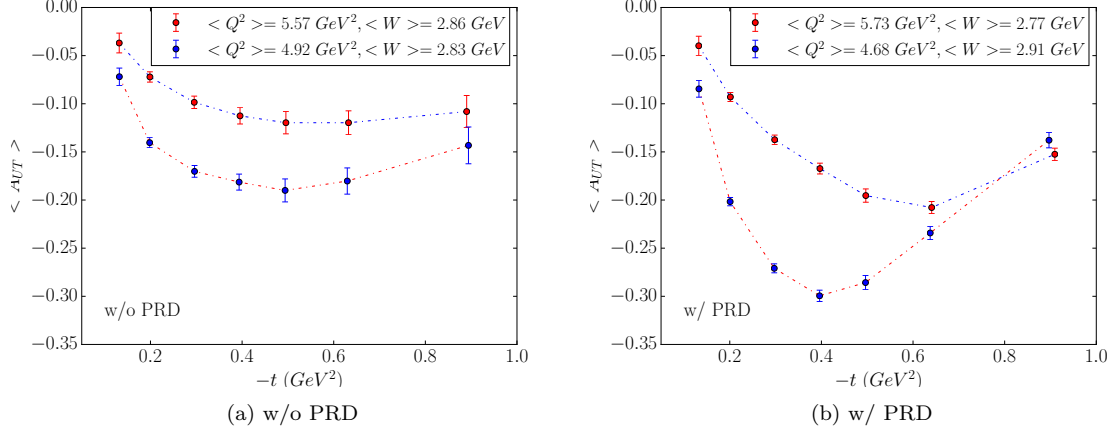

(a) w/o PRD

(b) w/ PRD

Figure 13: Projection of target sing spin asymmetry (A_{UT}) as a function of $-t$ for DEMP with transversely polarized ^{3}He at E_0=11 GeV (directly compared with Fig. 6). The data in each $-t$ bin are further divided into two Q^2 bins with similar statistics. The error bars are the projected statistical uncertainties defined in Eq. 10. The asymmetry value in each bin is predicted with the model given in Appendix-A and is diluted due to not separating the L/T contributions. The left plot shows the projection w/o a new proton recoil detector, while the right plot shows a better projected result with a new detector in addition. One can see the average asymmetries are also changed between two configurations and it is because the asymmetry strongly depends on Q^2 which changes w/ or w/o the PRD.

Fig. 13 shows the distribution of A_{UT} vs. $-t$ with projected statistical errors discussed above. Compared with the existing HERMES results (Fig. 6), the new measurement could provide more precision data to be directly compared with theoretical predictions. Extra binning on Q^2 enables us to study the Q^2-dependence of asymmetries as well as to constraint some corrections during the asymmetry extraction. The detailed information of each bin is listed in Table 4.

(a) w/o PRD

	t-bin#1	t-bin#2	t-bin#3	t-bin#4	t-bin#5	t-bin#6	t-bin#7
$<-t>$	0.13	0.20	0.30	0.40	0.50	0.63	0.89
Q^2 bin-set#1							
$<Q^2>$	4.12	4.44	4.92	5.40	5.87	6.43	7.31
$<\sigma_L/\sigma_T>$	6.17	5.19	4.24	3.59	3.00	2.23	1.08
$<f_{L/T}>$	0.79	0.77	0.74	0.71	0.67	0.60	0.41
$<A_{UT}>$	-7.20×10^{-2}	-1.40×10^{-1}	-1.70×10^{-2}	-1.81×10^{-1}	-1.90×10^{-1}	-1.80×10^{-1}	-1.19×10^{-1}
δA_{UT}	8.98×10^{-3}	5.20×10^{-3}	6.10×10^{-3}	8.30×10^{-3}	1.19×10^{-2}	1.36×10^{-2}	1.91×10^{-2}
N	3.44×10^4	1.02×10^5	7.38×10^4	3.98×10^4	1.93×10^4	1.48×10^4	7.55×10^3
Q^2 bin-set#2							
$<Q^2>$	4.36	4.91	5.58	6.16	6.62	7.13	7.80
$<\sigma_L/\sigma_T>$	6.74	6.32	5.76	5.12	4.29	3.14	1.66
$<f_{L/T}>$	0.80	0.79	0.78	0.76	0.73	0.66	0.51
$<A_{UT}>$	-3.69×10^{-2}	-7.22×10^{-2}	-9.85×10^{-2}	-1.13×10^{-1}	-1.20×10^{-1}	-1.20×10^{-1}	-1.08×10^{-1}
δA_{UT}	1.03×10^{-2}	5.35×10^{-3}	6.42×10^{-3}	8.44×10^{-3}	1.16×10^{-2}	1.24×10^{-2}	1.67×10^{-2}
N	2.63×10^4	9.70×10^4	6.72×10^4	3.89×10^4	2.07×10^4	1.81×10^4	9.94×10^3

(b) w/ PRD

	t-bin#1	t-bin#2	t-bin#3	t-bin#4	t-bin#5	t-bin#6	t-bin#7
$<-t>$	0.13	0.20	0.30	0.40	0.50	0.64	0.90
Q^2 bin-set#1							
$<Q^2>$	4.11	4.35	4.65	4.84	4.97	5.08	5.18
$<\sigma_L/\sigma_T>$	6.12	4.88	3.60	2.60	1.86	1.18	0.52
$<f_{L/T}>$	0.79	0.76	0.70	0.63	0.55	0.43	0.25
$<A_{UT}>$	-8.46×10^{-2}	-2.02×10^{-1}	-2.71×10^{-2}	-2.99×10^{-1}	-2.86×10^{-1}	-2.34×10^{-1}	-1.38×10^{-1}
δA_{UT}	8.62×10^{-3}	4.29×10^{-3}	4.66×10^{-3}	5.85×10^{-3}	$7.32 times 10^{-3}$	6.86×10^{-3}	7.91×10^{-3}
N	3.73×10^4	1.49×10^5	1.25×10^5	7.85×10^4	5.04×10^4	5.78×10^4	4.41×10^4
Q^2 bin-set#2							
$<Q^2>$	4.35	4.86	5.42	5.87	6.22	6.60	6.97
$<\sigma_L/\sigma_T>$	6.71	6.13	5.29	4.42	3.51	2.31	0.91
$<f_{L/T}>$	0.80	0.79	0.77	0.74	0.69	0.59	0.35
$<A_{UT}>$	-3.98×10^{-2}	-9.30×10^{-2}	-1.37×10^{-1}	-1.67×10^{-1}	-1.95×10^{-1}	-2.08×10^{-1}	-1.52×10^{-1}
δA_{UT}	9.92×10^{-3}	4.63×10^{-3}	4.83×10^{-3}	5.61×10^{-3}	6.91×10^{-3}	6.29×10^{-3}	6.35×10^{-3}
N	2.82×10^4	1.29×10^5	1.18×10^5	8.75×10^4	5.74×10^4	6.90×10^4	6.84×10^4

Table 4: Detailed information of projected bins from the new DEMP measurements with SoLID, while $<Q^2>$ and $<-t>$ are in the unit of GeV^2. The top (bottom) table is with respect to the case of proton detection w/o (w/) a new PRD. The data are divided into $14 -t$ bins in both $-t$ (7 bins) and $Q2$ (2 bins).

4 Missing Mass and Background

In the DEMP with a neutron, two charged particles, π^- and p, can be cleanly measured by the detector system. Moreover, the stuck proton will also be measured. Hence, contamination from other reactions, including DEMP with other two protons in ^3He, can be greatly eliminated. The dominant background

of the DEMP measurement comes from the SIDIS reactions of electrons scattering on the neutron and two protons in ^{3}He. In addition to detecting the recoil protons, which should largely suppress most of background, we will also rely on reconstructing the neutron missing mass spectrum to ensure the exclusivity of the DEMP events. In SIDIS, however, the final states include the scattered electron, the hadrons ($\pi^\pm$, $K^\pm$ etc.), as well as the undetected target fragments which could contain protons. Hence, the SIDIS events will possibly leak into the DEMP missing mass spectrum.

We studied the contamination of the SIDIS events in the DEMP missing momentum and mass spectra. The SIDIS reactions, $p(e, e'\pi^-)X$ and $n(e, e'\pi^-)X$, were simulated with the same generator used for the SoLID-SIDIS proposals, and their rates were calculated by matching the acceptance of scattered electrons and pions with the ones in DEMP. We then fold the SoLID detector resolutions into the spectra. Based on the current tracking study, the SoLID-SIDIS system can provide a momentum resolution of $2\%/\sqrt{E}$, a polar angle resolution of 0.6 mrad, an azimuthal angle resolution of 5 mrad and a vertex target position of 0.5 cm. It is difficult to estimate what percentage of the SIDIS target fragments contain protons, so we assumed the target fragments ("X") all contain one or more protons. Such an assumption likely results in the SIDIS background being significantly overestimated.

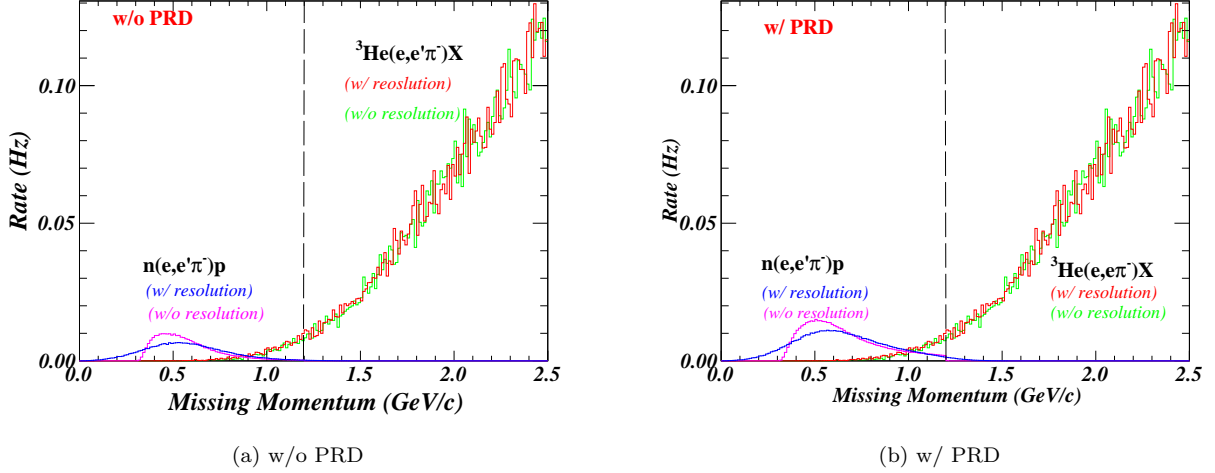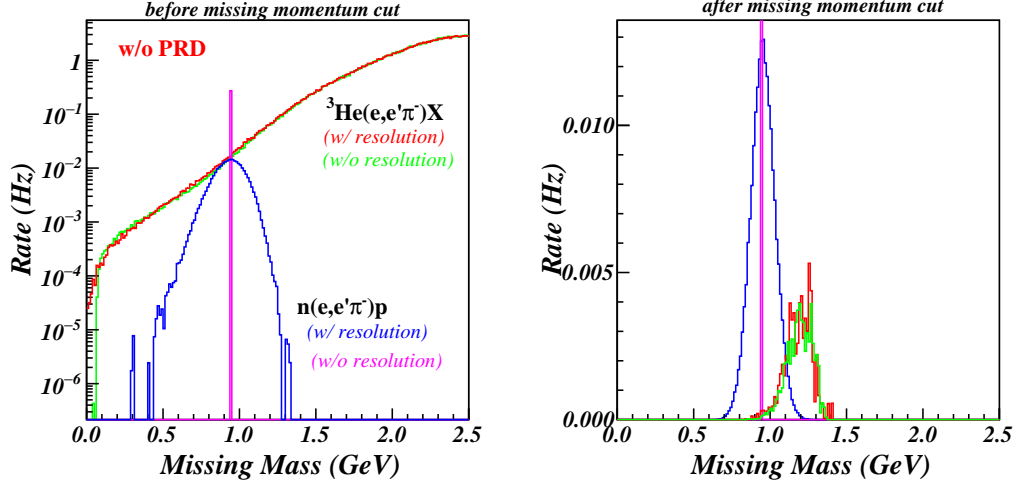(a) w/o PRD   (b) w/ PRD

Figure 14: Missing momentum spectra of DEMP and SIDIS events. The missing momentum distributes are well separated between two processes and one can apply a cut at $P_{miss} < 1.2$ GeV/c (indicated by the black dash line) to remove most of SIDIS events.

Shown in Fig. 14, we reconstruct the missing momenta of both processes. One immediately sees that the missing momentum distributions of two processes are well separated. The SIDIS background can be largely rejected when we apply a cut, $P_{miss} < 1.2$ GeV/c.

We then reconstructed the missing mass spectra of the DEMP and SIDIS events w/ and w/o the missing momentum cuts, as shown in Fig. 15. Before applying the missing momentum cut, the SIDIS background overwhelms the DEMP peak (note that the SIDIS rate is likely overestimated). After applying the cut, the DEMP peak dominates and the SIDIS background is largely suppressed. If we consider the fact that not every "X" in SIDIS contains a proton, the remaining background should be negligible.

Other random coincident background events will show up in the missing mass spectrum with more uniform

22

(a) w/o PRD
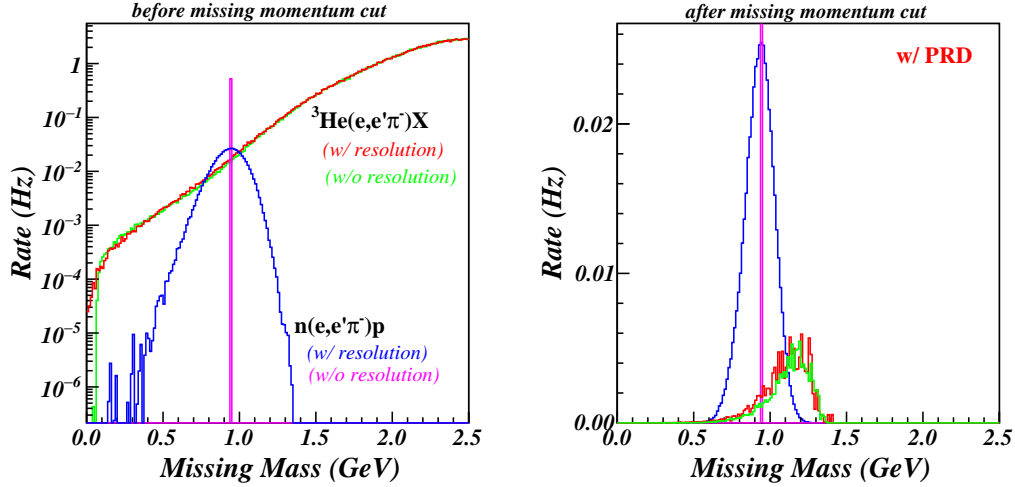
(b) w/ PRD

Figure 15: Missing mass spectra of DEMP and SIDIS events. Top (bottom) panel shows the missing mass distribution of DEMP events w/o (w/) proton detection by a new PRD. The left (right) plot of each panel shows the background contamination from SIDIS events before (after) the missing momentum cut shown in Fig. 14. The SIDIS background is already small compared with DEMP events. The actual SIDIS background should be much smaller, since we overestimated the SIDIS rate by assuming all target fragments ("X") in the SIDIS process contain protons.

distributions. We should be able to suppress most of them with tight missing momentum and missing mass cuts, and for these residuals that contaminate the real events, we are able to evaluate their asymmetries if nonzero, and apply corrections on the real asymmetry values. In general, we expect to have a clean measurement of the DEMP process because of all final particles being detected.

Sources	Relative Value
Beam Polarization	2%
Target Polarization	3%
Acceptance	3%
Other Contamination	$< 5\%$
Radiation Correction	1%

Table 5: Expected systematic errors.

5 Systematic Uncertainties

The detector related systematic errors are expected to be similar to the ones given in the E12-10-006 proposal as well as in other SIDIS experiments with SoLID. Here we list several major sources of systematic uncertainties as shown in Table 5.

6 Summary

The transverse single-spin asymmetry in the exclusive $\vec{n}(e, e'\pi^-)p$ reaction has been noted as being especially sensitive to the spin-flip generalized parton distribution (GPD) $\tilde{E}$. Factorization studies have indicated that precocious scaling is likely to set in at moderate $Q^2 \sim 2 - 4$ GeV^2, as opposed to the absolute cross section, where scaling is not expected until $Q^2 > 10$ GeV^2. Furthermore, this observable has been noted as being important for the reliable extraction of the charged pion form factor from pion electroproduction.

This measurement is complementary to a proposal to measure the longitudinal photon, transverse nucleon, single-spin asymmetry $A_L^{\perp}$ with the SHMS+HMS in Hall C [4]. The good resolution and reproducible systematic uncertainties of the SHMS+HMS setup allow the L–T separation needed to reliably measure this quantity. However, a wide $-t$ coverage is needed to obtain a good understanding of the asymmetry, and it always been intended to complement the SHMS+HMS $A_L^{\perp}$ measurement with an unseparated $A_{UT}^{sin(\phi-\phi_s)}$ measurement using a large solid angle detector. The high luminosity capabilities of SoLID make it well-suited for this measurement. Since an L–T separation is not possible with SoLID, the observed asymmetry is expected to be diluted by the ratio of the longitudinal cross section to the unseparated cross section. This was also true for the pioneering HERMES measurements, which provided a valuable constraint to models for the $\tilde{E}$ GPD. Our measurement will also help to constrain longitudinal backgrounds possibly complicating the extraction of the pion form factor from electroproduction experiment data, with the aim of eventually extending the kinematic range over which reliable F_π values can be acquired from electroproduction data.

A   Monte Carlo Model of Deep Exclusive π^- Production From The Neutron

Our Monte Carlo studies require a cross section model for an experimentally unexplored region of kinematics at larger values of Q^2, $-t$ and W. To briefly introduce the formalism, note that the scattering cross section for $n(e, e'\pi^-)p$ in one-photon exchange is given by equation 13:

$$\frac{d^5\sigma}{dE'd\Omega_{e'}d\Omega_\pi} = \Gamma_V \frac{d^2\sigma}{d\Omega_\pi}. \tag{13}$$

The virtual photon flux factor Γ_V in Eq. 13 is defined as:

$$\Gamma_v = \frac{\alpha}{2\pi^2} \frac{E'}{E} \frac{K}{Q^2} \frac{1}{1-\epsilon}, \tag{14}$$

where α is the fine structure constant, K is the energy of real photon equal to the photon energy required to create a system with invariant mass equal to W and ϵ is the polarization of the virtual photon.

$$K = (W^2 - M_p^2)/(2M_p) \tag{15}$$

$$\epsilon = \left(1 + \frac{2|\mathbf{q}|^2}{Q^2} \tan^2 \frac{\theta_e}{2}\right)^{-1}, \tag{16}$$

where θ_e is the scattering angle of scattered electron. The two-fold differential cross section $\frac{d^2\sigma}{d\Omega_\pi}$ in the lab frame can be expressed in terms of the invariant cross section in center of mass frame of photon and proton:

$$\frac{d^2\sigma}{d\Omega_\pi} = J \frac{d^2\sigma}{dtd\phi}, \tag{17}$$

where J is the transformation of coordinates Jacobian from lab Ω_π to t and ϕ (CM). The invariant cross section of Eq. 17 can be expressed in four terms. Two terms correspond to the polarization states of the virtual photon (L and T) and two states correspond to the interference of polarization states (LT and TT),

$$2\pi \frac{d^2\sigma}{dtd\phi} = \epsilon \frac{d\sigma_{\mathrm{L}}}{dt} + \frac{d\sigma_{\mathrm{T}}}{dt} + \sqrt{2\epsilon(\epsilon+1)}\frac{d\sigma_{\mathrm{LT}}}{dt} \cos\phi + \epsilon \frac{d\sigma_{\mathrm{TT}}}{dt} \cos 2\phi. \tag{18}$$

A.1   Data Constraints

Precise L/T separated experimental data of exclusive electroproduction of π^- on ^{2}H are available up to $Q^2 = 2.57$ GeV^2, $-t = 0.350$ GeV^2 and $W = 2.168$ GeV [33]. Precise L/T separated experimental data of exclusive electroproduction of π^+ on ^{1}H are available up to $Q^2 = 2.703$ GeV^2, $-t = 0.365$ GeV^2 and $W = 2.127$ GeV [25]. In Ref. [34] and Ref. [35], separated σ_L and σ_T are measured up to $Q^2 = 4.703$ GeV^2 and $W = 2.2$ GeV. CLAS experiment E99-105 measured the unseparated cross section at Q^2 up to 4.35 GeV^2 and $-t$ up to 4.5 GeV^2 [36]. The HERMES collaboration measured the unseparated cross section for Q^2=3.44 GeV^2 and 5.4 GeV^2 [37] at W=4 GeV.

A.2   Model for Higher Q^2 Kinematics

The electroproduction of exclusive charged pions is best described by the VR model [38]. The VR model is a Regge model with a parameterization of deep inelastic scattering amplitude to improve the description of σ_T. The description of σ_L is constrained by a fit to our Hall C data [25]. In Fig. 16, we plotted the last six data points of table v of Ref. [33], our parameterization and VR model points for exactly same values of Q^2, $-t$ and W. It shows the comparison of the same points of $\sigma_{L,T,LT,TT}$ vs. Q^2.
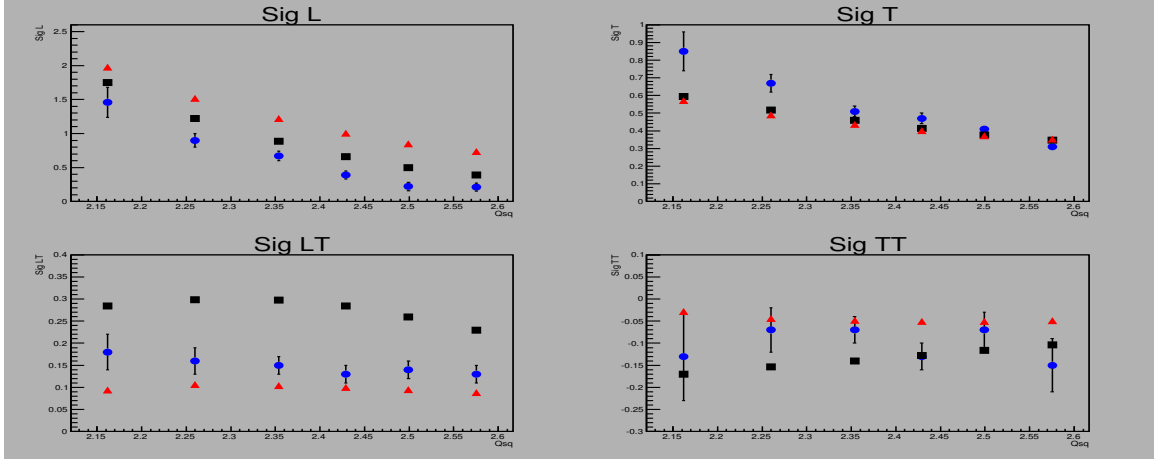

Figure 16: A π^- electroproduction comparison for the last six points of table v of Ref. [33], the VR model and our parameterization values vs. Q^2. Experimental data is shown in blue circles, VR model is shown in red triangles and our parameterization is shown in black boxes. In each graph, the value of $-t$ is decreasing left to right from maximum value 0.35 GeV^2 to 0.15 GeV^2. Value of W also decreases left to right from 2.30 GeV to 2.17 GeV.

A.3   Parameterization of σ_L, σ_T, σ_{LT}, & σ_{TT}

For exclusive DEMP in SoLID, the kinematic region of interest for this $\sigma_{L,T,LT,TT}$ parameterization is Q^2 from 4.5 GeV^2 to 7.5 GeV^2, $-t$ from 0 GeV^2 to 1.0 GeV^2, and we set $W = 3.0$ GeV. After the parameterization of $\sigma_{L,T,LT,TT}$ for $-t$ and Q^2, we used the same W dependence given by Ref. [25], which is $(W^2 - M^2)^{-2}$ where M is the proton mass. Our parameterization of all four cross sections is given in Eq. 19 to Eq. 22:

$$\sigma_L = \exp\left(P_1(Q^2) + |t| * P_1'(Q^2)\right) + \exp\left(P_2(Q^2) + |t| * P_2'(Q^2)\right) \tag{19}$$

$$\sigma_T = \frac{\exp\left(P_1(Q^2) + |t| * P_1'(Q^2)\right)}{P_1(|t|)} \tag{20}$$

$$\sigma_{LT} = P_5(t(Q^2)) \tag{21}$$

$$\sigma_{TT} = P_5(t(Q^2)), \tag{22}$$

where the parameters P_i are polynomial functions of ith order. Each coefficient (P_i) of fifth order equations Eq. 21 and Eq. 22 is a further second order polynomial of Q^2. Deep exclusive π^- events are generated using a C++ code. The quality of parameterization is checked by plotting the parameterization functions of $\sigma_{L,T,LT,TT}$ versus the VR model as shown in Fig. 17.
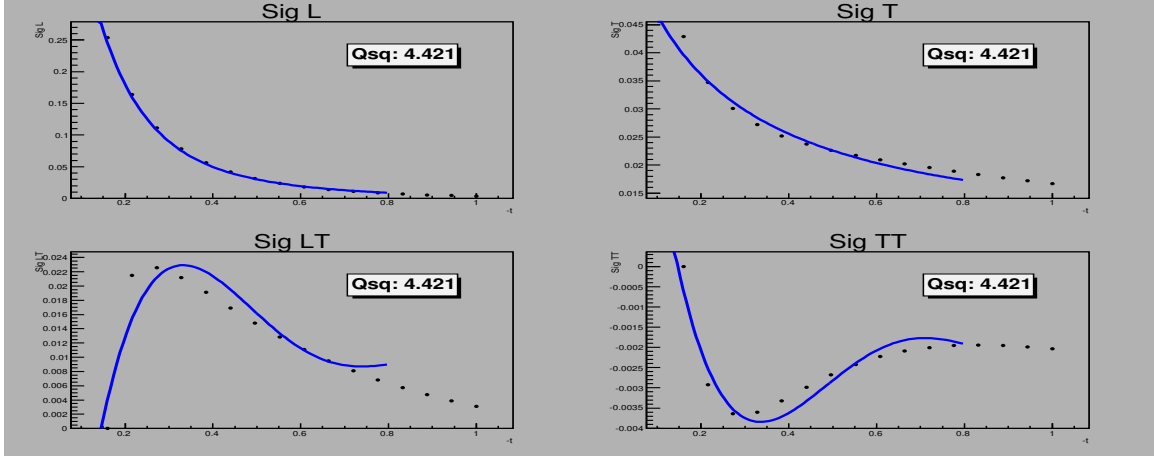

Figure 17: A comparison of parameterized $\sigma_{L,T,LT,TT}$ and VR model values at $Q^2=4.421$ GeV^2 and $W = 3.0$ GeV. Black points are VR model values and the blue line is the parameterized $\sigma_{L,T,LT,TT}$ given by equations Eq. 19 to Eq. 22.

A.4   Single Spin Asymmetry (SSA) $\mathbf{A_L^\perp}$

It is shown in Ref. [13] that the generalized parton distribution $(\tilde{E})$ can be probed by measuring the single spin asymmetry (SSA). The SSA is defined in Eq. 23

$$\mathbf{A_L^\perp} = \frac{\int_0^\pi \mathbf{d}\beta \frac{\mathbf{d}\sigma_L^{\pi^-}}{\mathbf{d}\beta} - \int_\pi^{2\pi} \mathbf{d}\beta \frac{\mathbf{d}\sigma_L^{\pi^-}}{\mathbf{d}\beta}}{\int_0^{2\pi} \mathbf{d}\beta \frac{\mathbf{d}\sigma_L^{\pi^-}}{\mathbf{d}\beta}}, \tag{23}$$

where β is the angle between the transversely polarized target vector and the reaction plane, and $\sigma_L^{\pi^-}$ is the exclusive π^- cross section for longitudinal virtual photons.

We parameterized the single spin asymmetry using the model of Ref. [15] at $x = 0.1$ and $x = 0.3$, as given in Eq. 24

$$\mathbf{A_L^\perp} = \begin{cases} A_0 \left[1 - \exp^{[-\lambda \times (t - t_{min})]} \right] & \text{if } t \geq t_{min}, \\ 0 & \text{if } t < t_{min}. \end{cases} \tag{24}$$

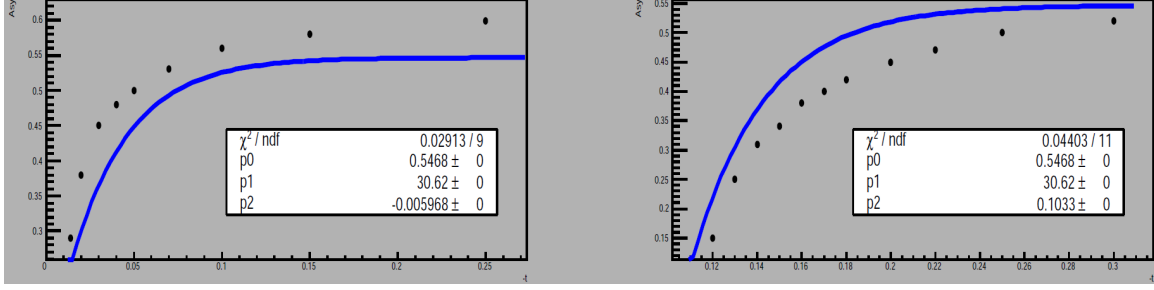The SSA parameterization is compared to the model of Ref. [15] in Fig. 18.

Figure 18: Parameterization of single spin asymmetry $\mathbf{A_L^\perp}$ vs. $-t$ at $x = 0.1$ (left) and $x = 0.3$ (right), where the points are from the model defined in Ref. [15] and blue line is our parameterization function.

B Proton Recoil Detector

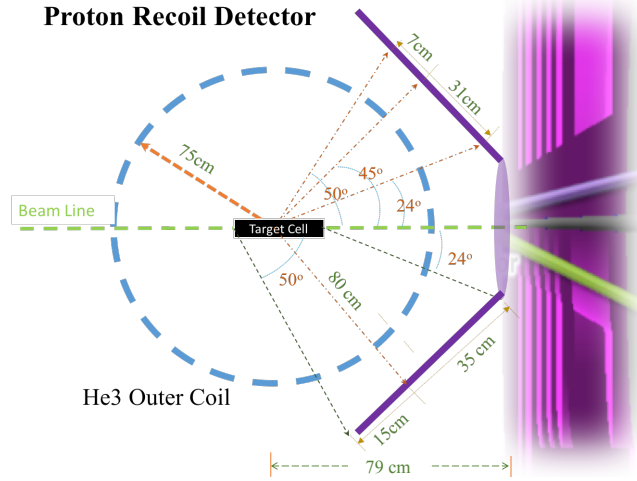## B.1 Requirements and Conceptual Design

Figure 19: Scheme of the new proton recoil detector. Such a cone-shape detector will be placed outside the outer Helmholtz coil of the ^{3}He target system, covering polar angles from $24°$ to $50°$ and with 2π acceptance in azimuthal angle. We assume the detector plane to be tilted by $-45°$ w.r.t. the beam direction with the vertical distance from the target center to the detector to be around 80 cm. In this setting, the length of the detector is about 38 cm, and considering the target cell is 20 cm long, we extend the length to be 50 cm. The inner and outer radius to be near 32 cm and 67 cm, respectively. The rough location of the solenoid is also indicated here. Note that lengths and locations are rough estimated, and the scales of angles and length are not proportional to the real scales.

As shown in Fig. 19, a new proton recoil detector (PRD) will be placed right outside the ^{3}He target system where the radius of the outer Helmholtz coil is about 75 cm. The PRD will need to cover the polar angle from $24°$ to $50°$ and provide full acceptance in azimuthal angle. To minimize the detector area, the detector plane is tilted by $-45°$ along the beam direction and the vertical distance from the plane to the target center is about 80 cm. After taking into account that the target cell is 20 cm long, we require the length of the detector to be 50 cm, and its inner and outer radii to be 32 cm and 67 cm, respectively.

To successfully select protons, we require the timing resolution of the detector to be better than 60 ps,

as discussed in Section 2.3. Since the detector is close to the target and will suffer a huge background of low energy particles, particularly low energy electrons, the detector will be divided into fine segments to avoid pile-up of background signals. In addition, a thin aluminum sheet of ∼4.5 mm thickness in front of the detector should be able to block most of low energy particles. The rough angular information provided by this detector will be helpful to further reject background and isolate protons during the offline data analysis when reconstructing missing mass and momentum.

B.2   Scintillating Fiber Tracker

One of the good candidates for the PRD is a scintillating fiber tracker (SFT) [39]. Scintillating fibers (SciFi) have now been largely used in experiments of particle physics because of its fast timing response and flexibility, and several commercial manufacturers are able to produce high quality fibers and at relatively low prices. Instead of using traditional large paddles, we can construct the PRD by grouping SciFi in arrays and form the detector planes. With two planes of fibers at perpendicular directions, the PRD can also provide position information by determining which fiber is fired in each plane. A 1-mm round fiber is able to provide a 0.5 mm position resolution and with a distance of 80 cm away from the target center, the angular resolution can be better than 0.5 mrad, which can be essential to further isolate protons and reduce background. On top of that, the SciFi is highly segmented so the rate of random low energy background particles hitting on a single fiber can be largely minimized, and the pile-up effect should be significantly reduced compared with large area scintillator paddles.

We will choose silicon photo-multipliers (SiPM) as the photon-detectors to collect light produced in the fibers. SiPM is idea for low-photon-number counting since the light yield produced by a SciFi is not as strong as one produced in a thin scintillator paddle. It is also not sensitive to magnetic field, while the PRD will be placed in between the target system and the SoLID magnet which both have strong magnetic field. Besides, there will be a lot of read out channels and the price of SiPM is low enough to make the new detector affordable. The combination of SciFi and SiPM will make the PRD a very compact detector which is very important since the space between the target system and the solenoid magnet is limited.

A prototype project, funded by JSA postdoctoral fellow award [39], has been under development and we expect to build a small SFT and test its performance near a target system with electron beam at JLab.

References

[1] Approved SoLID SIDIS experiment E12-10-006, "Target Single Spin Asymmetry in Semi-Inclusive Deep-Inelastic $(e, e'\pi^{\pm})$ Reaction on a Transversely Polarized ^{3}He Target at 11 GeV", $https : //www.jlab.org/exp\_prog/proposals/14/E12 - 10 - 006A.pdf$

[2] SoLID Collaboration, "Solenoial Large Intensity Device Preliminary Conceptual Design Report," $http : //hallaweb.jlab.org/12GeV/SoLID/files/solid\_precdr.pdf$

[3] A. Airapetian, Phys. Lett. **B 682** (2010) 345-350, arXiv:0907.2596 [hep-ex].

[4] PR12-12-005: D. Dutta, D. Gaskell, W. Hersman, G.M. Huber, et al., "The Longitudinal Photon, Transverse Nucleon, Single-Spin Asymmetry in Exclusive Pion Production".

[5] M. Diehl, Contribution to the eRHIC White Paper, arXiv:hep-ph/0010200.

[6] J.C. Collins, L. Frankfurt, M. Strikman, Phys. Rev. D **56** (1997) 2982.

[7] K. Goeke, M.V. Polyakov, M. Vanderhaeghen, Prog. Part. Nucl. Phys. **47** (2001) 401-515.

[8] A.V. Radyushkin, arXiv:hep-ph/0101225.

[9] A.W. Thomas, W. Weise, "The Structure of the Nucleon", J. Wiley-VCH, 2001.

[10] R.E. Marshak, Riazuddin, C.P. Ryan, "Theory of Weak Interactions in Particle Physics", J. Wiley, 1969.

[11] M. Penttinen, M.V. Polyakov, K. Goeke, Phys. Rev. C **62** (2000) 014024 1-11.

[12] A.V. Belitsky, D. Mueller, Phys. Lett. **B 513** (2001) 349-360.

[13] L.L. Frankfurt, P.V. Pobylitsa, M.V. Polyakov, M. Strikman, Phys. Rev. D **60** (1999) 014010 1-11.

[14] M. Vanderhaeghen, P.A.M. Guichon, M. Guidal, Phys. Rev. D **60** (1999) 094017 1-28.

[15] L.L. Frankfurt, M.V. Polyakov, M. Strikman, M. Vanderhaeghen, Phys. Rev. Lett. **84** (2000) 2589-2592.

[16] A.V. Belitsky, CIPANP 2003 proceedings. arXiv: hep-ph/0307256.

[17] L. Mankiewicz, G. Piller, A. Radyushkin, Eur. Phys. J. **C 10** (1999) 307-312.

[18] C.E. Carlson, J. Milana, Phys. Rev. Lett. **65** (1990) 1717.

[19] E12-06-101, "Measurement of the Charged Pion Form Factor to High Q^2", G.M. Huber, D. Gaskell, spokespersons.

[20] A. Bartl, W. Majerotto, Nucl. Phys. **B62** (1973) 267-285.

[21] S. V. Goloskokov and P. Kroll, Eur. Phys. J. C **65**, 137 (2010), arXiv:0906.0460 [hep-ph].

[22] M. Diehl, S. Sapeta, Eur. Phys. J. C **41** (2005) 515, arXiv:hep-ph/0503023.

[23] pCDR for the Science and Experimental Equipment for the 12 GeV Upgrade of CEBAF, June, 2004. V. Burkert et al., PAC18 Review of the Science Driving the 12 GeV Upgrade, July, 2000.

[24] S. V. Goloskokov and P. Kroll, private communications 2009-12.

[25] H.P. Blok, et al., Phys. Rev. C **78** (2008) 045202.

[26] Approved SoLID SIDIS experiment E12-11-007, "Asymmetries in Semi-Inclusive Deep-Inelastic $(e, e'\pi^{\pm}$ Reactions on a Longitudinally Polarized ^{3}He Target at 8.8 and 11 GeV", $https : //www.jlab.org/exp_prog/PACpage/PAC37/proposals/Proposals/New\%20Proposals/PR - 11 - 007.pdf$

[27] Approved SoLID SIDIS experiment E12-11-108, "Target Single Spin Asymmetry in Semi-Inclusive Deep-Inelastic $(e, e'\pi^{\pm}$ Reactions on a Transversely Polarized Proton Target", $https : //www.jlab.org/exp\_prog/proposals/11/PR12 - 11 - 108.pdf$

[28] Approved SoLID J/ψ experiment E12-12-006A, "Near Threshold Electroproduction of J/ψ at 11 GeV", $https : //www.jlab.org/exp_prog/proposals/12/PR12 - 12 - 006.pdf$

[29] Approved SoLID SIDIS experiment E12-10-006A, "Dihadron Electroproduction in DIS with Transversely Polarized ^{3}He Target at 11 and 8.8 GeV", $https : //www.jlab.org/exp_prog/proposals/14/E12 - 10 - 006A.pdf$

[30] Approved SoLID SIDIS experiment E12-11-108A, "Target Single Spin Asymmetry Measurements in the Inclusive Deep-Inelastic $vecN(e, e')$ Reaction on Transversely Polarized Proton and Neutron (^{3}He) Targets using the SoLID Spectrometer" $https : //www.jlab.org/exp_prog/proposals/14/E12 - 11 - 108A_E12 - 10 - 006A.pdf$

[31] Approved SoLID PVDIS experiment E12-10-007, "Precision Measurement of Parity-violation in Deep Inelastic Scattering Over a Broad Kinematic Range", $https : //www.jlab.org/exp\_prog/PACpage/PAC37/proposals/Proposals/Previously\%20Approved/E12 - 10 - 007.pdf$

[32] J. L. Friar et al., Phys. Rev. C 42, (1990) 2310; C. Ciofi degli Atti, and S. Scopetta, Phys. Lett. **B404**, (1997) 223; R.W. Schulze and P.U. Sauer, Phys. Rev. **C56** (1997) 2293; F. Bissey, A.W. Thomas, and I.R. Afnan, Phys. Rev. **C64**, (2001) 024004.

[33] G. M. Huber *et al.*, Phys. Rev. **C91**, 015202 (2015).

[34] T. Horn *et al.*, Phys. Rev. Lett **97**, 192001 (2006).

[35] T. Horn *et al.*, Phys. Rev. **C78**, 058201 (2008).

[36] http://clas.sinp.msu.ru/cgi-bin/jlab/db.cgi?eid=36;search=on

[37] A. Airapetian *et al.*, Phys. Lett. B. **659**, (2008).

[38] T. Vrancx and J. Ryckebusch., Phys. Rev. **C89**, 025203 (2014).

[39] Z. Ye, A Prototype Project of a new Scintillating Fiber Tracker, 2014 JSA Postdoctoral Fellowship, "$https : //userweb.jlab.org/\ yez/Work/SFT/SFT\_prop.pdf$"